Mixed alkali and alkaline-earth borate $Li_2Sr_4B_{12}O_{23}$ single crystal

A.H. Reshak

New Technologies – Research Centre, University of West Bohemia, Univerzitni 8, 306 14 Pilsen, Czech Republic
Center of Excellence Geopolymer and Green Technology, School of Material Engineering, University Malaysia Perlis, 01007 Kangar, Perlis, Malaysia

A B S T R A C T

A comprehensive theoretical investigation of the electronic band structure, density of states, electron charge density distribution and the optical properties for mixed alkali and alkaline-earth borate $Li_2Sr_4B_{12}O_{23}$ (LSBO) single crystals were performed. The experimental geometrical structure was optimized by minimizing the forces acting on each atom. Calculations were performed using the full potential linear augmented plane wave plus local orbitals (*FPLAPW + lo*) method within the local density approximation (*LDA*), generalized gradient approximation (*GGA*) and the recently modified Becke–Johnson potential (*mBJ*). Our calculations show that LSBO crystal is a direct band gap semiconductor. The calculated band gap is 4.64 eV (*LDA*), 4.92 eV (*GGA*) and 5.51 eV (*mBJ*). An earlier calculation using the CASTEP code within *LDA* obtained a band gap of about 4.66 eV. To overcome the well-known *LDA* underestimation of the energy gap we have used *GGA* and *mBJ*. We find that *mBJ* succeed by large amount in bringing the calculated bond lengths in good agreement with the experimental data. Also we found that using *mBJ* to calculate the optical properties gives a birefringence of about 0.068 (at λ = 586.5 nm) in excellent agreement with the experimental data (0.068 at λ = 586.5 nm). Therefore, we believe that the *mBJ* calculations reported here show excellent agreement with the experimental data.

1. Introduction

The formation of a large variety of borates is a consequence of two unique coordination of B atoms BO_3 and BO_4. Borates are promising candidates for several applications. Several borates materials considered to be as potential candidates for generating second harmonic in the ultra-violet region [1–3] among them is the alkali or alkaline-earth metal borates. The cations of these alkali or alkaline-earth metal borates favor excellent optical transparency in the ultra-violet region [4]. Some alkali/alkaline earth metal borates, $Li_2Sr_4B_{12}O_{23}$ (LSBO) [5,6], have a three-dimensional framework and can be used as micro-porous materials. Recently Zheng and Li [7] have used the high-temperature solid state reaction to synthesize a pure mixed alkali–alkaline earth metal borate of $Li_2Sr_4B_{12}O_{23}$ with micro-porous structure. The single crystal was characterized by XRD, FT-IR, TG techniques, and chemical analysis. Zhang et al. [6] have used the top-seeded solution growth method below 730 °C to grow ternary lithium strontium borate $Li_2Sr_4B_{12}O_{23}$ single crystals with size 20 × 10 × 4 mm. They found that $Li_2Sr_4B_{12}O_{23}$ crystallizes in the monoclinic space group P21/c. Using the IR spectrum they confirm the presence of both BO_3 and BO_4 groups. Furthermore, they

calculate the electronic band structure and the density of states using the *ab initio* density functional theory (DFT) method implemented in the CASTEP package within the local density approximates (LDA). It has been found that the calculated energy band gap of LSBO is about 4.66 eV. Also they have calculated the birefringence, imaginary and real parts of the optical dielectric function using LDA.

It is well-known that in calculating the self-consistent band structure within DFT, the LDA approximation underestimates the energy band gap by around 10–30% [8–10]. This is mainly due to the fact that LDA has simple forms that are not sufficiently flexible to accurately reproduce both the exchange–correlation energy and its charge derivative. Therefore, we thought it is worthwhile to do more accurate calculations using full potential method with different exchange and correlation potentials. We would like to mention that we are not aware of experimental data for the energy gap of LSBO crystal. However, since there is an experimental value for the birefringence of LSBO therefore, we have performed calculations using three different exchange-correlation potentials in order to ascertain which one gives the birefringence in close agreement with the experimental value. We feel that the exchange-correlation which will succeed in bringing the calculated birefringence in close agreement with the experimental value, would also give the correct band gap. First-principles calculation is one powerful and useful tool to predict the crystal structure and

E-mail address: maalidph@yahoo.com

properties related to the electron configuration of a material before its synthesis [11–15].

2. Details of calculations

$Li_2Sr_4B_{12}O_{23}$ (LSBO) single crystal is alkali and alkaline-earth metal mixed borate with $[B_{10}O_{18}]^{6-}$ network and isolated $[B_2O_5]^{4-}$ unit. LSBO crystallizes in a monoclinic structure, space group, $P2_1/c$. The unit cell parameters are $a = 6.4664(4)$ Å, $b = 8.4878(4)$ Å and $c = 15.3337(8)$ Å, $\beta = 102.02(3)°$, $V = 823.13(8)$ Å^3, $Z = 2$ [6]. The crystal structure of LSBO is shown in Fig. 1(a)–(c). In this calculation we have used the crystallographic data obtained by Zhang et al [6]. Using GGA [16] the atomic coordinates of LSBO were optimized by minimization of the forces acting on each atom. We assume that the structure is fully relaxed when the forces on the atoms reach values less than (1 mRy/a.u.). The optimized atomic positions along with those obtained from the crystallographic data [6] were listed in Table 1, good agreement was found. Once the forces are minimized in this construction one can then find the self-consistent density at these positions by turning off the relaxations and driving the system to self-consistency. From the obtained relaxed geometry the electronic structure, chemical bonding, electronic charge density and the optical properties have been determined and compared with the available experimental data.

The calculation were performed using DFT within the full potential linear augmented plane wave plus local orbitals (FPLAPW + lo) method in a scalar relativistic version as embodied in the WIEN2k code [17]. The exchange-correlation (XC) potential was solved using three different possible approximations. The XC are described by LDA [18] and GGA, which is based on exchange-correlation energy optimization to calculate the total energy. In addition, we have used the recently modified Becke–Johnson potential (mBJ) [19] which optimizes the corresponding potential for electronic band structure calculations. It is well-known that in calculating the self-consistent band structure within DFT, the LDA approximation underestimates the energy band gap by around 10–30% [8–10]. This is mainly due to the fact that LDA has simple forms that are not sufficiently flexible to accurately reproduce both the exchange–correlation energy and its charge derivative. To overcome this drawback we proposed mBJ. The mBJ, a modified Becke–Johnson potential, allows the calculation of band gaps with accuracy similar to the very expensive GW calculations [19,15]. It is a local approximation to an atomic "exact-exchange" potential and a screening term. Since the exact value of the experimental band gap is not reported in the literature, therefore based on our previous calculation [20–22] of the band gap using mBJ for several systems whose energy band gap are known experimentally, in those previous calculations we found very good agreement with the experimental data. Thus, we believe that our calculations reported in this paper would produce very accurate and reliable value of the energy band gap.

The Kohn–Sham equations are solved using a basis of linear APW's. The potential and charge density in the muffin-tin (MT) spheres are expanded in spherical harmonics with $l_{max} = 8$ and non-spherical components up to $l_{max} = 6$. In the interstitial region the potential and the charge density are represented by Fourier series. Self-consistency is obtained using 300 $\bar{k}$ points in the
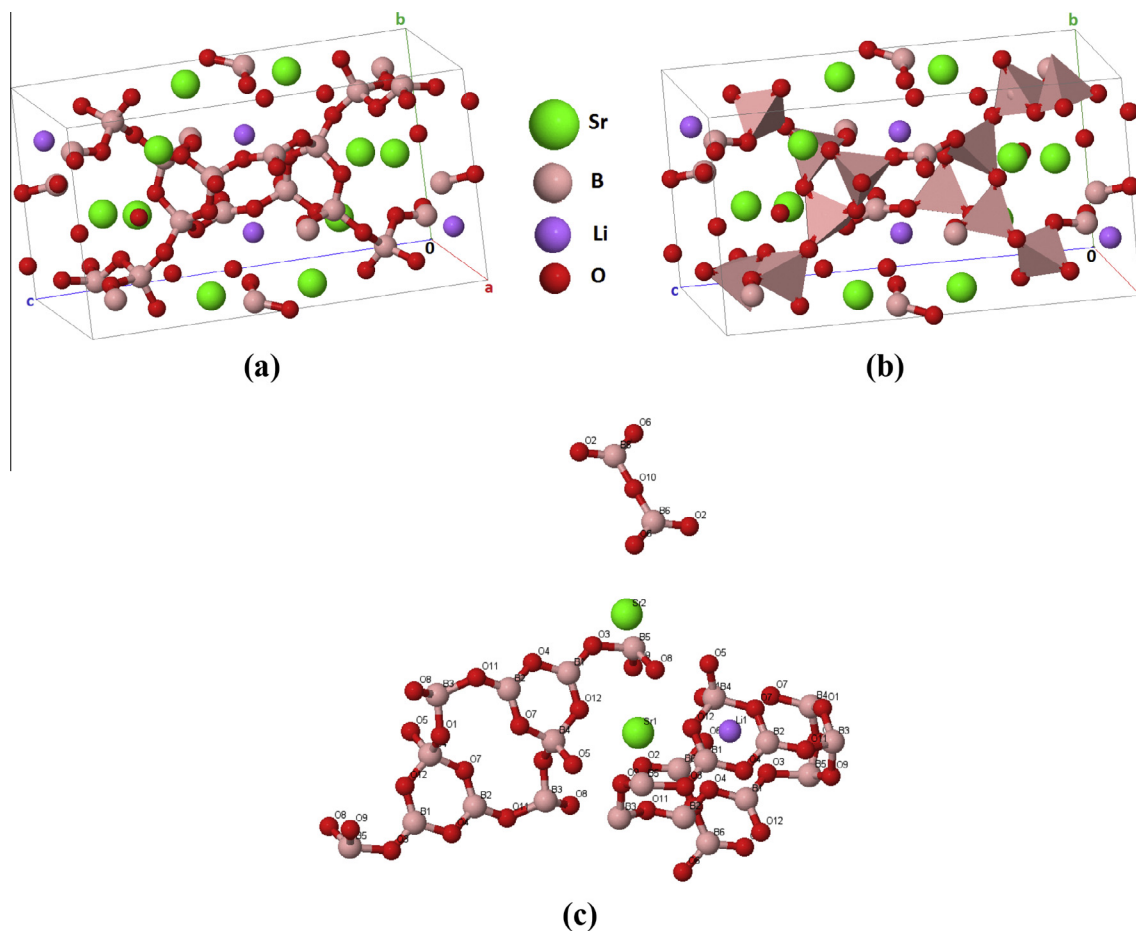
Fig. 1. (a) and (b) Different view for the unit cell of LSBO single crystal; (c) LSBO molecule.

Table 1
Calculated atomic positions in comparsion with the experimental data [6].

Atom	x-exp.	x-opt.	y-exp.	y-opt.	z-exp.	z-opt.
Li(1)	0.6591(10)	0.6569	0.3052(7)	0.3044	0.5243(3)	0.5250
Sr(1)	1.03080(4)	0.0314	0.32574(3)	0.3254	0.725982(18)	0.7262
Sr(2)	0.60025(5)	0.6095	0.48279(3)	0.4827	0.885128(18)	0.8864
B(1)	0.9342(6)	0.9340	0.1549(4)	0.1530	0.9228(2)	0.9236
B(2)	1.2477(6)	0.2475	0.3276(4)	0.3284	0.5384(2)	0.5392
B(3)	1.5240(6)	0.5243	0.3786(4)	0.3789	0.6832(2)	0.6836
B(4)	1.2837(6)	0.2845	0.1034(4)	0.1038	0.8817(2)	0.8822
B(5)	0.5760(6)	0.5758	0.1621(4)	0.1828	0.8076(2)	0.8076
B(6)	0.0971(6)	0.0976	0.5386(4)	0.5397	0.9270(3)	0.9263
O(1)	0.6711(3)	0.6707	0.4377(2)	0.4376	0.62997(14)	0.6296
O(2)	1.0229(4)	0.0240	0.0277(3)	0.0301	0.65581(16)	0.6573
O(3)	0.7240(3)	0.7219	0.1760(2)	0.1749	0.90176(14)	0.9027
O(4)	1.0283(3)	0.0270	0.3358(3)	0.3367	0.51380(14)	0.5152
O(5)	1.3698(3)	0.3688	0.2082(2)	0.2095	0.82412(14)	0.8241
O(6)	0.2999(3)	0.3049	0.5843(3)	0.5846	0.94881(15)	0.9484
O(7)	0.3648(3)	0.3656	0.3498(3)	0.3492	0.47627(14)	0.4770
O(8)	0.6460(3)	0.6494	0.2731(3)	0.2749	0.74875(14)	0.7503
O(9)	1.4201(4)	0.4213	0.5026(2)	0.5033	0.72428(14)	0.7253
O(10)	0.0000	0.0000	0.5000	0.5000	1.0000	0.0000
O(11)	1.3376(3)	0.3373	0.2885(3)	0.2882	0.62370(14)	0.6255
O(12)	1.0494(3)	0.04865	0.1233(3)	0.1232	0.86022(14)	0.8602

irreducible Brillouin zone (*IBZ*). We have calculated the electronic band structure, density of states, electronic charge density distribution and linear optical properties using 500 $\bar{k}$ points in the *IBZ*. The self-consistent calculations are converged since the total energy of the system is stable within 0.00001 Ry.

3. Results and discussion

3.1. Electronic band structure and density of states

To ascertain the effect of exchange correlation on the value of the energy band gap, three different types of exchange correlation potentials were employed. Fig. 2(a)–(c) illustrates the calculated electronic band structure within *LDA*, *GGA* and *mBJ*. It is clear that the exchange correlation has significant influence on the conduction bands and hence on the energy gap value. Moving from $LDA \rightarrow GGA \rightarrow mBJ$ cause to shift the conduction band minimum (CBM) toward higher energies by around 0.3 eV ($LDA \rightarrow GGA$) and

0.6 eV ($GGA \rightarrow mBJ$) keeping the valence band maximum fixed at Fermi level. In all cases the Fermi level is at 0.0 eV. The electronic band structure shows that the CBM and the VBM are situated at the center of BZ resulting in a direct band gap in agreement with the previous results using CASTEP code within LDA [6]. Our calculated value of the energy gap is about 4.64 eV (*LDA*), 4.92 eV (*GGA*) and 5.51 eV (*mBJ*) in comparison with the previous calculation using CASTEP within *LDA* (4.66 eV) [6]. The *mBJ* normally brings the calculated energy gap close to the experimental data. Since the exact value of the experimental band gap is not reported in the literature, therefore based on the available experimental value of the birefringence [6] and our experiences with using *mBJ* [20–22], we expect good agreement with the experimental data.

Further investigation to ascertain the effect of exchange correlation on the electronic structure and hence on the value of the energy band gap, we have calculated total density of states (*TDOS*) as illustrated in Fig. 3(a) which confirms there is a significant influence on the band/state dispersion when one moves from $LDA \rightarrow GGA \rightarrow mBJ$. The *TDOS* support our previous finding from
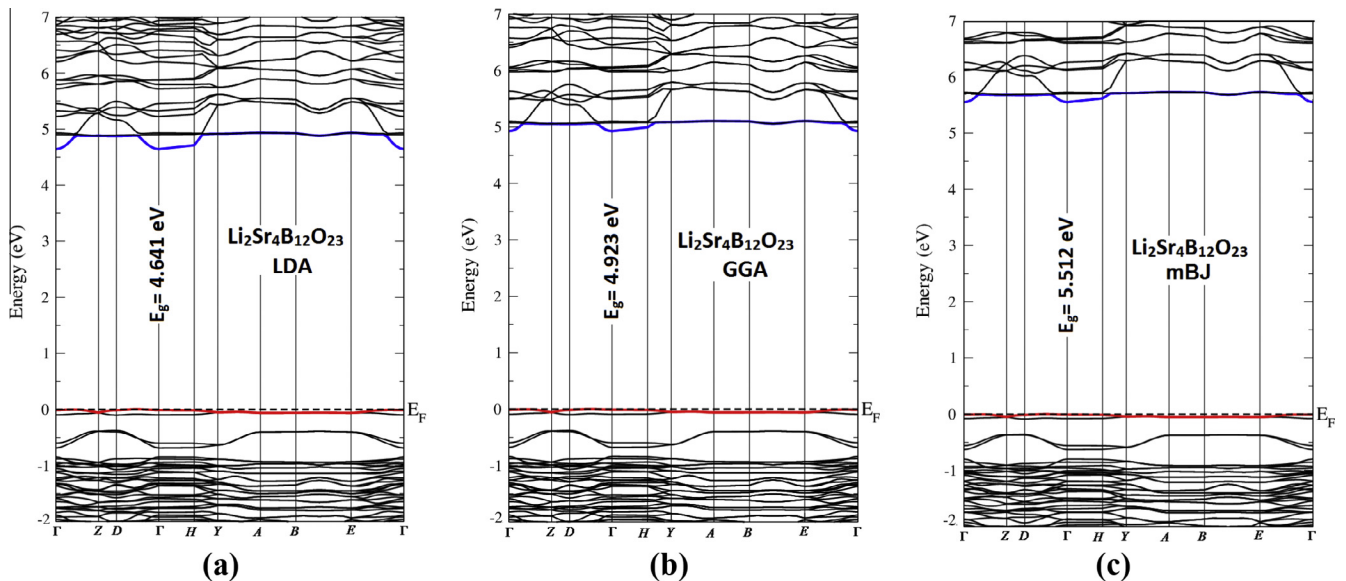
Fig. 2. The calculated electronic band structure of LSBO using three different types of exchange correlation potentials LDA, GGA and mBJ.
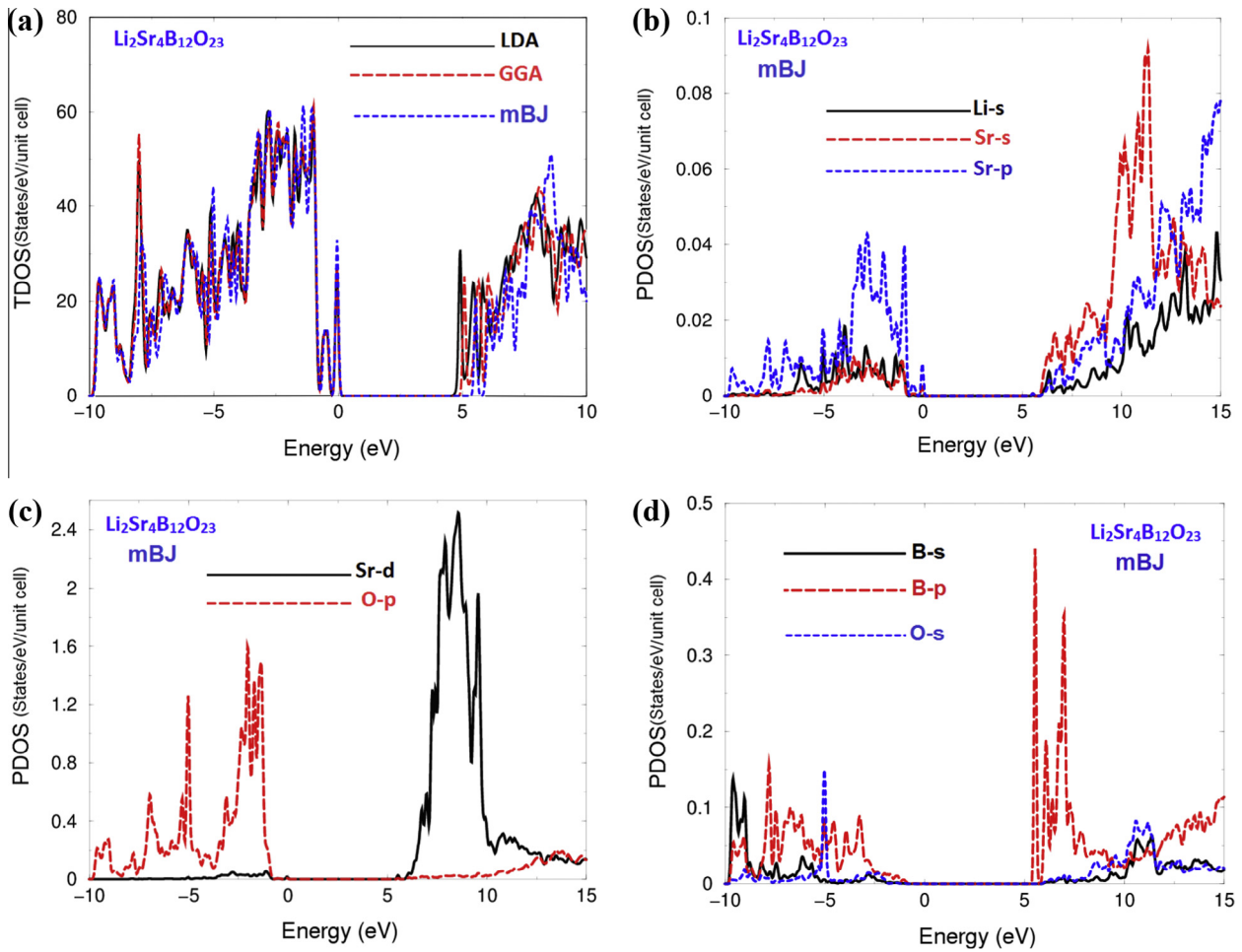
Fig. 3. (a) Calculated total density of states (states/eV/unit cell) using LDA, GGA and EVGGA; (b) calculated partial density of states (states/eV/unit cell) using mBJ.
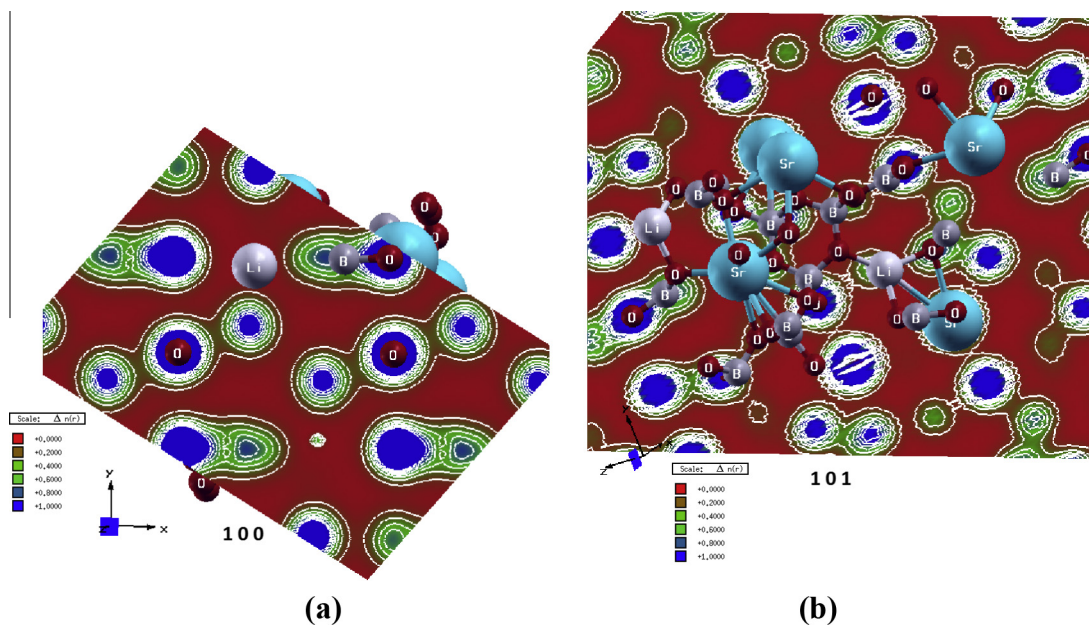
Fig. 4. The electron charge density distribution were calculated for; (a) (1 0 0) crystallographic plane and (b) (1 0 1) crystallographic plane.

the electronic band structure that the *CBM* shift toward higher energies resulting in increasing the band gap's value, and *mBJ* causes to increase the band gap value by around 0.87 eV over the value obtained from *LDA*. Therefore, we choose *mBJ* to calculate the partial density of states (*PDOS*). The Li-s, Sr-s/p/d, B-s/p and O-s/p partial density of states are shown in Fig. 3(b)–(d). From

Table 2
Calculated bond lengths in comparsion with the experimental data [6].

Bonds	Exp. bond lengths (Å)	Calc. bond lengths (Å)	Bonds	Exp. bond lengths (Å)	Calc. bond lengths (Å)
$Li-O_6$	1.926(7)	1.911	B_1-O_2	1.342(4)	1.340
$Li-O_7$	1.929(7)	1.913	B_1-O_{12}	1.358(4)	1.351
$Li-O_1$	1.961(6)	1.962	B_1-O_4	1.404(4)	1.400
$Li-O_3$	2.014(6)	2.017	B_2-O_7	1.349(4)	1.337
Sr_1-O_2	2.570(2)	2.566	B_2-O_{11}	1.357(4)	1.348
Sr_1-O_5	2.586(2)	2.579	B_2-O_4	1.392(4)	1.389
Sr_1-O_8	2.622(2)	2.618	B_3-O_8	1.450(4)	1.448
Sr_1-O_1	2.656(2)	2.649	B_3-O_9	1.460(4)	1.457
Sr_1-O_{12}	2.665(2)	2.660	B_3-O_1	1.465(4)	1.460
Sr_1-O_2	2.746(3)	2.739	B_3-O_{11}	1.553(4)	1.549
Sr_1-O_{11}	2.791(2)	2.788	B_4-O_5	1.444(4)	1.440
Sr_1-O_{12}	2.847(2)	2.840	B_4-O_1	1.455(4)	1.449
Sr_1-O_9	2.936(2)	2.912	B_4-O_7	1.489(4)	1.481
Sr_1-O_4	3.251(2)	3.248	B_4-O_{12}	1.492(4)	1.489
Sr_2-O_6	2.502(2)	2.511	B_5-O_9	1.441(4)	1.442
Sr_2-O_9	2.504(2)	2.500	B_5-O_8	1.441(4)	1.442
Sr_2-O_6	2.557(2)	2.548	B_5-O_5	1.462(4)	1.463
Sr_2-O_{11}	2.634(2)	2.621	B_5-O_3	1.562(4)	1.559
Sr_2-O_2	2.668(3)	2.659	B_6-O_6	1.341(4)	1.338
Sr_2-O_3	2.721(2)	2.719	B_6-O_2	1.347(5)	1.349
Sr_2-O_8	2.808(2)	2.800	B_6-O_{10}	1.431(4)	1.430
Sr_2-O_{10}	2.812(3)	2.809			
Sr_2-O_5	2.819(2)	2.811			

the *PDOS* we can identify the angular momentum characters of various structures.

The energy region extended from -10.0 eV up to Fermi energy (E_F) mainly originates from O-p state with small contribution by B-s/p and O-s states. The energy region from the CBM and above is formed by Sr-d with small admixture of O-s, Li-s and Sr-s/p states. The VBM is mainly from by Sr-p and O-p states and the CBM by Sr-d and O-s states. It is clear that there is a strong/weak hybridization between the states below and above E_F. It has been found that in the energy range between -5.0 eV and E_F the B-s state hybridized with O-s state. While in the energy region extended from -3.0 eV up to E_F the Li-s state hybridized with B-s and O-s states. In the conduction band, Li-s hybridized with B-s in two regions the first one is extended from the CBM up to 10.5 eV and the second one between 11.5 and 13.0 eV. The degree of the hybridization indicates the chemical bonding characters. Based on above we can say that there exists a mixture of covalent and ionic bonding.

To support this statement we have taken a careful look at valence band's electronic charge density distribution to visualize the charge transfer and the chemical bonding characters. We have calculated the total valence charge density distribution in (100) and (101) crystallographic planes as shown in Fig. 4(a) and (b). The crystallographic plane (100) exhibit a uniform spherical charge surrounding the O atoms indicating the ionic characters of O atoms. The contour plots of charge density between B and O atoms indicate a strong covalent bonding between B and O atoms. According to Pauling scale the electro-negativity of Li, Sr, B and O atoms are 0.98, 0.95, 2.04 and 3.44, respectively. Therefore, if the electro-negativity difference between the atoms is grater than 1.7 the bonds are ionic while if it is less than 1.7 the bonds exhibit covalent characters. Due to the high electro-negativity of O atoms we can see charge transfer toward O atoms as indicated by the blue color (according to the thermoscale the blue color exhibit the maximum charge). The (101) crystallographic plane confirm the existence of the covalent bonding between B and O atoms. The calculated bond lengths between Li and the four O atoms vary between 1.90 and 2.1 Å in good agreement with the measured values 1.926(7)–2.014(6) Å [6]. Further information from (101) crystallographic plane, the Sr1 atoms are linked to ten O atoms to form the polyhedra Sr_1O_{10}, nine out of ten are strongly linked to Sr1 and the tenth O atom is linked to Sr1 by weak bond. The bond lengths of the nine Sr–O vary

between 2.51 and 2.90 Å. These values are in good agreement with the measured one (2.570(2)–2.936(2) Å) [6], the length of the weak bond is about 3.21 Å in good agreement with the measured value 3.251(2) Å [6]. Also one can see each Sr2 atom is bonded to nine O atoms to form Sr_2O_9 polyhedra, the calculated bond lengths vary between 2.49–2.79 Å which show good agreement with the measured (2.502(2)–2.819(2) Å [6]. The calculated bond lengths show good agreement with the measured bond lengths [6] in Table 2.

3.2. Linear optical properties

Further deep insight into the electronic structure can be obtained by calculating the optical properties. From the imaginary and real parts of the optical dielectric function, the refractive indices can be calculated. From the imaginary part of the optical dielectric function one can directly estimate the optical gap, whereas it is indirectly estimated from the real part of the optical dielectric function and the refractive indices, both of $\varepsilon_1(0)$ and $n(0)$ ($n = \sqrt{\varepsilon}$) are inversely proportional with the energy gap. This could be explained on the basis of the Penn model [23]. Penn proposed a relation between $\varepsilon(0)$ and E_g, $\varepsilon(0) \approx 1 + (\hbar\omega_P/E_g)^2$. E_g is some kind of averaged energy gap which could be related to the real energy gap. This motivated us to calculate the optical properties to seek the corrected value of the energy band gap. Since *mBJ* is expected to bring the calculated energy band gap close to the experimental one, therefore by using *mBJ* we expected the electric-dipole transitions will occurs between the exact valence and the conduction bands to allow the valid optical transition. It is well known that the exact form of exchange-correlation functional is unknown. Therefore the accuracy of our results will be sensitive to selection of the exchange-correlation functional and it can play a major role for the accuracy of the results and this is one of the main drawbacks in DFT.

The monoclinic symmetry allows five non-zero components of the second-order optical dielectric tensor. These are $\varepsilon^{xx}(\omega)$, $\varepsilon^{xy}(\omega)$, $\varepsilon^{yy}(\omega)$, $\varepsilon^{yx}(\omega)$ and $\varepsilon^{zz}(\omega)$. In order to identify the structures of these components we need to look at the magnitude of the optical matrix elements. The observed structures of $\varepsilon^{xy}(\omega)$ and $\varepsilon^{yx}(\omega)$ would correspond to those transitions that have very small optical
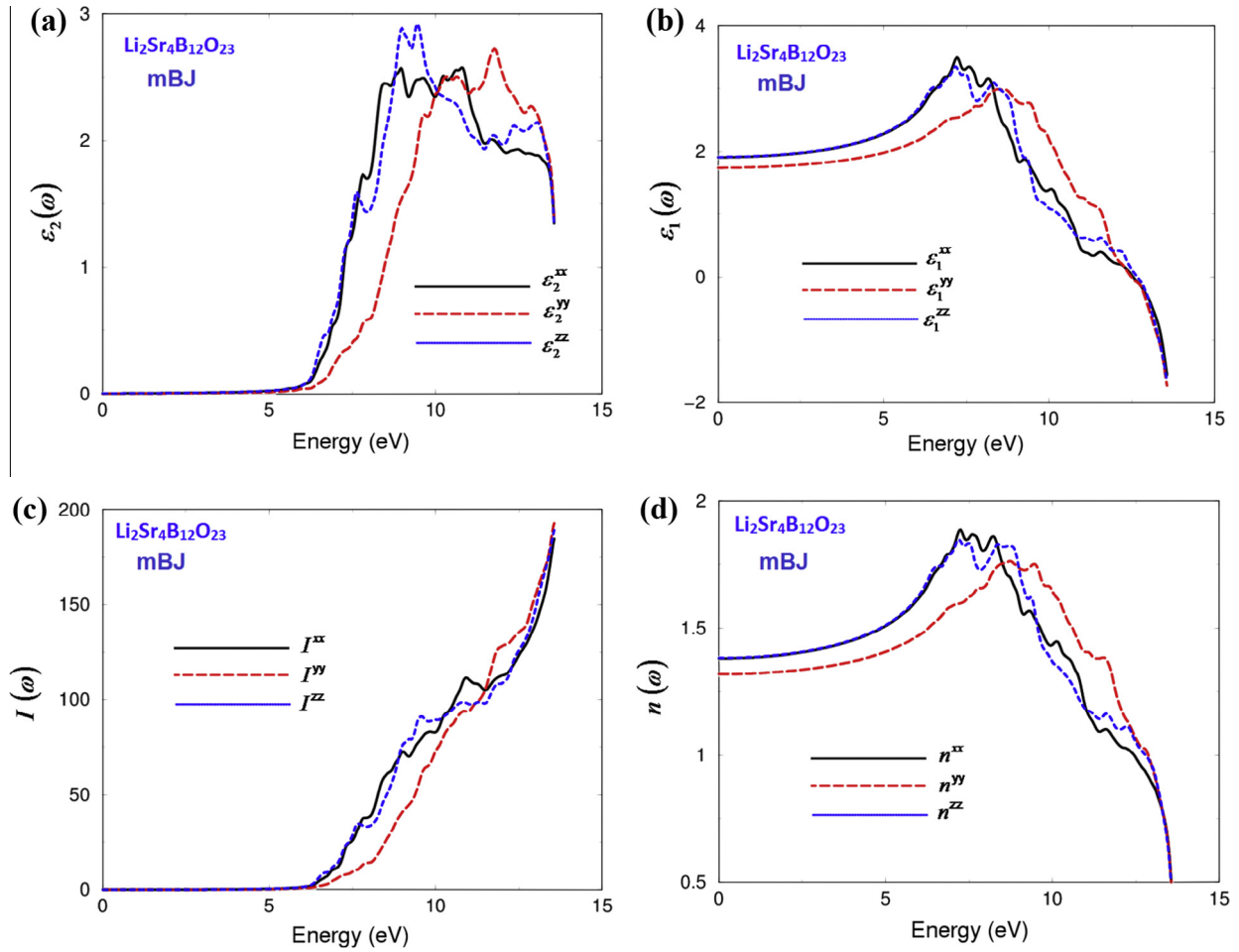
Fig. 5. (a) Calculated $\varepsilon_2^{xx}(\omega)$ (**dark solid curve-black color online**), $\varepsilon_2^{yy}(\omega)$ (light dashed curve-red color online) and $\varepsilon_2^{zz}(\omega)$ (light dotted curve-blue color online) spectra. (b) Calculated $\varepsilon_1^{xx}(\omega)$ (**dark solid curve-black color online**), $\varepsilon_1^{yy}(\omega)$ (light dashed curve-red color online) and $\varepsilon_3^{zz}(\omega)$ (light dotted curve-blue color online) spectra. (c) Calculated $I^{xx}(\omega)$ (**dark solid curve-black color online**), $I^{yy}(\omega)$ (light dashed curve-red color online) and $I^{zz}(\omega)$ (light dotted curve-blue color online) spectra. The absorption coefficient in 10^4 s^{-1}. (d) Calculated $n^{xx}(\omega)$ (**dark solid curve-black color online**), $n^{yy}(\omega)$ (light dashed curve-red color online) and $n^{zz}(\omega)$ (light dotted curve-blue color online) spectra. (For interpretation of the references to color in this figure legend, the reader is referred to the web version of this article.)

Table 3
Calculated $\varepsilon_1^{xx}(0)$, $\varepsilon_1^{yy}(0)$, $\varepsilon_1^{zz}(0)$, $n^{xx}(\omega)$, $n^{yy}(\omega)$, $n^{zz}(\omega)$ and $\Delta n(\omega)$.

	LDA		GGA		mBJ	
	At static limit	At λ = 586.5 nm	At static limit	At λ = 586.5 nm	At static limit	At λ = 586.5 nm
$\varepsilon_1^{xx}(0)$	2.257	2.333	2.164	2.232	1.906	1.954
$\varepsilon_1^{yy}(0)$	2.1035	2.161	2.005	2.055	1.739	1.772
$\varepsilon_1^{zz}(0)$	2.261	2.337	2.167	2.235	1.910	1.958
$\varepsilon_1^{tot}(0)$	2.207	2.277	2.112	2.174	1.851	1.894
$\delta\varepsilon$	−0.070	−0.076	−0.076	−0.082	−0.091	−0.097
$n^{xx}(\omega)$	1.502	1.527	1.471	1.494	1.381	1.398
$n^{yy}(\omega)$	1.450	1.470	1.416	1.433	1.319	1.331
$n^{zz}(\omega)$	1.504	1.529	1.472	1.495	1.382	1.400
$\Delta n(\omega)$	0.053	0.058,0.066[a]	0.0555	0.0615	0.625	0.068, 0.068[b]

[a] Ref. [6]; the calculated value of $\Delta n(\omega)$ at λ = 586.5 nm.
[b] Ref. [6]; the experimental value of $\Delta n(\omega)$ at λ = 586.5 nm.

matrix elements. Therefore, we will concentrate only on the dominate components correspond to the transitions that have large optical matrix elements i.e. $\varepsilon^{xx}(\omega)$, $\varepsilon^{yy}(\omega)$ and $\varepsilon^{zz}(\omega)$ which are correspond to [100], [010] and [001] polarization directions. Thus, the imaginary part $\varepsilon_2^{xx}(\omega)$, $\varepsilon_2^{yy}(\omega)$ and $\varepsilon_2^{zz}(\omega)$ of the optical function's dispersion are completely define the linear optical properties. These originate from inter-band transitions between valence and conduction bands.

The expression for calculating the imaginary part of the optical dielectric functions are given elsewhere [24]. Fig. 5(a) exhibits the imaginary part of the optical function's dispersion. The broadening is taken to be 0.1 eV which is typical of the experimental accuracy. The edge of optical absorption (fundamental absorption edge) for $\varepsilon_2^{xx}(\omega)$, $\varepsilon_2^{yy}(\omega)$ and $\varepsilon_2^{zz}(\omega)$ are located at 5.52 eV. These edges of optical absorption give the threshold for direct optical transitions between the top of valence (Sr-p and O-p states) band and bottom

of conduction band (Sr-d and O-s states). $\varepsilon_2^{xx}(\omega)$, $\varepsilon_2^{yy}(\omega)$ and $\varepsilon_2^{zz}(\omega)$ exhibit the main spectral structure at 10.0, 12.0 and 9.0 eV respectively. These main spectral structures are due to the optical transitions between Li-s, Sr-s/p/d, B-s/p and O-s/p states of the valence bands to O-s/p, Li-s, Sr-s/p, B-s/p and O-s states of the conduction bands. There is considerable anisotropy between $\varepsilon_2^{xx}(\omega) \sim \varepsilon_2^{zz}(\omega)$ and $\varepsilon_2^{yy}(\omega)$ indicating that LSBO is an almost uniaxial crystal. With the aid of the Kramers–Kronig transformation [25] the real parts of the optical dielectric functions can be obtained from the imaginary parts. Fig. 5(b) illustrates the three components $\varepsilon_1^{xx}(\omega)$, $\varepsilon_1^{yy}(\omega)$ and $\varepsilon_1^{zz}(\omega)$. The vanishing frequency value of the dielectric function defines the static electronic dielectric constant. The vanishing frequency values along with the values at $\lambda = 586.5$ nm are presented in Table 3, from these value one can derive the uniaxial anisotropy $\delta\varepsilon = [(\varepsilon_0^{II} - \varepsilon_0^{\perp})/\varepsilon_0^{tot}]$ which is found to be -0.070, -0.076 and -0.091 for LDA, GGA, mBJ, respectively. These values show the influence of the exchange correlation potential on the optical properties. Thus, the larger $\varepsilon_1(0)$ value is corresponding to the small energy gap. Hence a larger E_g yields a smaller $\varepsilon(0)$. As it has been mentioned above this could be explained on the basis of the Penn model [23]. From the calculated imaginary and real parts of the optical function's dispersion one can obtain the absorption coefficient $I(\omega)$ and the refractive indices $n(\omega)$.

The absorption coefficient $I(\omega)$ of LSBO is illustrated in Fig. 5(c), it shows that the edge of optical absorption (fundamental absorption edge) are located at 5.52 eV which confirms our previous observation from Fig. 2(a). Beyond the optical absorption edge there is a rapid and sharp absorption to reach its maximum value at a round 14.0 eV. The calculated refractive indices as shown in Fig. 5(d) confirm the existence of considerable anisotropy. $n(0)$ is inversely proportional with the energy gap. Therefore, one can derive the value of the energy gap from $n(0)$ on the basis of the Penn model. From the calculated values of $n^{xx}(\omega)$, $n^{yy}(\omega)$ and $n^{zz}(\omega)$ one can calculate the birefringence $\Delta n(\omega)$. The value the $\Delta n(\omega)$ and the corresponding values of the refractive indices are listed in Table 3, in comparison with the experimental value and other theoretical value (LDA – CASTEP) of $\Delta n(\omega)$ [6]. We find that our calculated $\Delta n(\omega) = 0.068$ is in excellent agreement with the measured value (0.068) [6] and slightly better than the one calculated by LDA – CASTEP (0.066).

4. Conclusions

The calculated electronic band structure shows that the CBM and VBM are located at the center of the BZ resulting in a direct band gap. The previous calculation of Zhang's group using CASTEP code within LDA gave an energy gap of 4.64 eV. To overcome the LDA underestimate of the energy gap we have used the recently modified Becke–Johnson potential (mBJ) which succeed by large amount in bringing the calculated birefringence (0.068) close to the experimental data (0.068). Therefore, we expected our calculated energy gap (5.51 eV) using mBJ is in close agreement with the expected experimental band gap. Future experimental work will testify our calculated results. The mBJ, a modified Becke–Johnson potential, allows the calculation of band gaps with accuracy similar to the very expensive GW calculations. It is a local approximation to an atomic "exact-exchange" potential and a screening term. As there is no information about the experimental gap therefore, based on our experiences with mBJ we hope our work will result in such measurements. We have calculated the total and partial density of states, electronic charge density distribution and the optical properties. The calculated partial density of states helps to identify the angular momentum character of the various structures and the hybridizations between the states to identify the bonding nature. The contour plots of charge density indicate the accumulations of charge around O atoms, and the bonds characters depending on Pauling electro-negativity difference between the atoms. The calculated bond lengths show good agreement with the experimental data.

References

[1] P. Becker, Adv. Mater. 10 (1998) 979.
[2] T. Sasaki, Y. Mori, M. Yoshimura, Y.K. Yap, T. Kamimura, Mater. Sci. Eng. 30 (2000) 1.
[3] S.L. Pan, J.P. Smit, B. Watkins, M.R. Marvel, C.L. Stern, K.R. Poeppelmeier, J. Am. Chem. Soc. 128 (2006) 11631.
[4] C. Chen, Z. Lin, Z. Wang, Appl. Phys. B: Lasers Opt. 80 (2005) 1.
[5] Z.H. Liu, R.B. Zhang, Microporous material for strontium lithium borate and its preparation method and application, 28–26, CN 102517625 A.
[6] Min Zhang, Shilie Pan, Jian Han, Zhihua Yang, Su Xin, Wenwu Zhao, J. Solid State Chem. 190 (2012) 92–97.
[7] Wenjie Zheng, Dawei Li, J. Therm. Anal. Calorim. 117 (2014) 439–442.
[8] P. Dufek, P. Blaha, K. Schwarz, Phys. Rev. B 50 (1994) 7279.
[9] Yan Zhao, Donald G. Truhlar, J. Chem. Phys. 130 (2009) 074103.
[10] Hai Xiao, Jamil Tahir-Kheli, William A. Goddard, J. Phys. Chem. Lett. 2 (3) (2011) 212–217.
[11] A.H. Reshak, I.V. Kityk, S. Auluck, J. Alloy. Compd. 460 (2008) 99–102.
[12] Y. Saeed, S. Nazir, A.H. Reshak, A. Shaukat, J. Alloy. Compd. 508 (2010) 245–250.
[13] A.H. Reshak, H. Kamarudin, S. Auluck, J. Alloy. Compd. 509 (2011) 9685–9691.
[14] Hardev S. Saini, Mukhtiyar Singh, A.H. Reshak, Manish K. Kashyap, J. Alloy. Compd. 536 (2012) 214–218.
[15] R.I. Eglitis, Int. J. Mod. Phys. B 28 (2014) 1430009.
[16] J.P. Perdew, S. Burke, M. Ernzerhof, Phys. Rev. Lett. 77 (1996) 3865.
[17] P. Blaha, K. Schwarz, G.K.H. Madsen, D. Kvasnicka, J. Luitz, WIEN2k, An Augmented Plane Wave Plus Local Orbitals Program for Calculating Crystal Properties, Vienna University of Technology, Austria, 2001.
[18] W. Kohn, L.J. Sham, Phys. Rev. A 140 (1965) 1133.
[19] F. Tran, P. Blaha, Phys. Rev. Lett. 102 (2009) 226401.
[20] A.H. Reshak, H. Kamarudin, S. Auluck, J. Mater. Sci. 48 (2013) 1955–1965.
[21] A.H. Reshak, I.V. Kityk, O.V. Parasyuk, A.O. Fedorchuk, Z.A. Alahmed, N. AlZayed, H. Kamarudin, S. Auluck, J. Mater. Sci. 48 (2013) 1342–1350.
[22] A.H. Reshak, I.V. Kityk, O.V. Parasyuk, H. Kamarudin, S. Auluck, J. Phys. Chem. B 117 (2013) 2545–2553.
[23] D.R. Penn, Phys. Rev. B 128 (1962) 2093.
[24] F. Bassani, G.P. Parravicini, Electronic States and Optical Transitions in Solids, Pergamon Press Ltd., Oxford, 1975.
[25] H. Tributsch, Z. Naturforsch. A 32A (1977) 972.